Stability of Drug-Induced Tubulin Rings by Fluorescence Correlation Spectroscopy

Hacène Boukari,* Ralph Nossal, and Dan L. Sackett

Laboratory of Integrative and Medical Biophysics, National Institute of Child Health and Human Development, National Institutes of Health, Bethesda, Maryland 20892

Received August 27, 2002; Revised Manuscript Received November 26, 2002

ABSTRACT: Fluorescence correlation spectroscopy (FCS) was applied to investigate the stability of tubulin rings that result from the interaction of αβ-tubulin dimers with three vinca domain-binding peptides—cryptophycin 1, hemiasterlin, and dolastatin 10. These peptides inhibit tubulin polymerization into microtubules and, instead, induce the formation of single-walled tubulin rings of 23.8 nm mean diameter for cryptophycin and 44.6 nm mean diameter for hemiasterlin and dolastatin, as revealed by electron microscopy on micromolar drug−tubulin samples. However, the hydrodynamic diameter and the apparent number of fluorescent particles, determined from analysis of FCS measurements obtained from nanomolar drug−tubulin samples, indicate variation in the stability of the rings depending on the drug and the tubulin concentration. Cryptophycin−tubulin rings appear to be the most stable even with tubulin concentration as low as 1 nM, whereas hemiasterlin−tubulin rings are the least, depolymerizing even at relatively high concentrations (100 nM). In contrast, the dolastatin−tubulin rings demonstrate an intermediate level of stability, depolymerizing significantly only at tubulin concentrations below 10 nM. We also compare the stability results with those of cytotoxicity measurements taken on several cell lines and note a rough correlation between the cytotoxicity of the drugs in cell cultures and the stability of the corresponding drug-induced rings.

Microtubules are a major component of the cytoskeleton and comprise a central element of the mitotic apparatus of the cell. As such, these dynamic polymers have been targeted in nature by many small molecules that organisms have evolved to achieve ecological advantages. A number of these natural products have been developed into clinically useful agents. While some are among the oldest known drugs in continual use (such as colchicine), the detailed mechanism of action of these agents continues to be a focus of research ((*1*) and references therein). Although all of these agents bind to the αβ-heterodimeric tubulin subunit of microtubules, some agents preferentially bind to the polymerized form and others to the unpolymerized, dimeric form. The structural consequences of drug binding range from hyperstabilization of microtubules, to depolymerization of microtubules, to induction of aberrant nonmicrotubule polymers.

Currently, a new class of antimitotic natural compounds is being evaluated for use in the treatment of neoplastic disease. These compounds are small peptides and depsipeptides, which often exhibit potent cytotoxicity and antimicrotubule activity (for review, see ref *2*). In vitro, these compounds, which include cryptophycin, hemiasterlin, and dolastatin, depolymerize microtubules, causing, instead, αβ-tubulin dimers to assemble into closed, single-walled ring-like nanostructures (*3*, *4*). In the case of cryptophycin, the predominant ring is composed of eight dimers, and its mean diameter is close to 23.8 nm (*5*). Hemiasterlin and dolastatin rings contain 14 tubulin dimers, and their diameters are close to 44.8 nm. These results were obtained from several related measurements involving dynamic light scattering, analytical ultracentrifugation, and electron microscopy (*3*−*5*). In these investigations, appropriate pH, salt concentrations and, more pointedly, relatively high concentrations of tubulin (typically 10 μM concentrations) and stoichiometric excess of drug were used to ensure the formation and stability of the rings.

In light of the potent cytotoxicity of these compounds it is desirable to understand the stability of the drug−tubulin complexes at lower concentrations. Yet, traditional analytical methods such as light scattering, turbidity, and ultracentrifugation are subject to technical and sample-related factors that impose limitations and hinder interpretation of measurements. Moreover, electron microscopy, which can provide structural information on sparse samples, involves procedures that may disturb the target macromolecular complexes.

Some of these difficulties can be alleviated by using fluorescent techniques to obtain information about the inter- and intramolecular interactions as well as motions of specific targets (*6*−*13*). In particular, fluorescence correlation spectroscopy (FCS) has been applied successfully to investigate biological samples at nanomolar concentrations (see refs *12* and *13* and examples therein). FCS uses statistical fluctuations in the fluorescence intensity of a small illuminated sample volume to study macromolecules or supramolecular complexes moving in and out of the volume. The measured fluctuations are correlated in time, and the resulting time-delayed correlation function provides measures of the concentration and the translational diffusion coefficient of the fluorescent targets. FCS can probe femtoliter volumes

* Corresponding author. Address: LIMB/NICHD, Bldg 9, Room 1E116, 9 Memorial Drive, Bethesda, MD 20892. Phone: 301-594-0359. Fax: 301-480-2030. E-mail: boukarih@mail.nih.gov.

[1] Abbreviations: FCS, fluorescence correlation spectroscopy; MAP, microtubule-associated protein; PIPES, piperazine-*N*,*N*′-bis(2-ethanesulfonic acid); BSA, bovine serum albumin.

10.1021/bi026751q
Published on Web 01/15/2003

of solution, making the technique appropriate for studying solutions with nanomolar concentrations of fluorescent targets. For example, the technique was recently applied to investigate the binding kinetics of colchicine to tubulin (*14*) and the exchange of tubulin dimers with microtubules (*15*).

Our aim in the present investigation is to study the stability of tubulin polymers induced by the interaction of cow-brain tubulin with the three small molecules already mentioned: the depsipeptide cryptophycin 1 (isolated from cyanobacteria (*16*−*20*)), the tripeptide hemiasterlin (isolated from marine sponges (*21*−*24*)), and the tetrapeptide dolastatin 10 (isolated from shell-less mollusks (*23*, *25*−*27*)). We focus on a specific set of conditions in which tubulin is lowered to nanomolar concentrations, and determine the stability of the drug−tubulin polymer rings. From the measured correlation functions we determine the translational diffusion time of the fluorescent particles, enabling us to infer sizes of polymer entities such as rings and/or other macromolecular entities, and to compare them with the known diameters of stable rings. We also determine how the apparent number of fluorescent particles in the excitation volume depends on the tubulin concentration. This dependence is examined and compared with the calculated ratios based on the numbers of tubulin dimers in the drug−tubulin polymer rings (8 for cryptophycin and 14 for hemiasterlin and dolastatin). We analyze both measured parameters—the hydrodynamic diameter and the apparent number—to assess the stability of the rings as the tubulin solution was diluted to nanomolar scale. We find that cryptophycin−tubulin rings are the most stable rings, maintaining their structure even at 1 nM concentration of tubulin whereas the hemiasterlin−tubulin rings are the least, dissociating into smaller polymer entities (likely linear hexamers) even at 100 nanomolar tubulin concentration. The dolastatin−tubulin rings have an intermediate behavior, depolymerizing from the stable ring structure only at relatively low concentrations of tubulin ($\leq$10 nM).

We have also compared the cytotoxicity of these compounds in several cancer cell lines representing different tissues of origin. All three compounds are potently cytotoxic, exhibiting subnanomolar IC50 values, but their relative cytotoxicity varies by more than a factor of 20. The relative cytotoxicity appears to correlate with the relative stability of the drug-induced ring polymers.

MATERIALS AND METHODS

A. Calibration. For testing and calibration of the FCS setup, we acquired from Molecular Probes (Eugene, Oregon) highly monodisperse (44 and 104 nm diameter) fluorescent carboxylated-modified polystyrene spheres (catalog numbers: F8792 and F8800 respectively with Ex/Em: 540/560 nm) and single-isomer 5-carboxytetramethylrhodamine (TAMRA catalog number: C6121 Ex/Em:542/568). In addition to the information provided by the company, we applied dynamic light scattering to determine the translational diffusion coefficient, and hence the size of the fluorospheres as well as the dispersity in size of the particles (10% for 44 nm and 6% for 104 nm). TAMRA molecules (M_w = 430) were particularly useful to calibrate the FCS setup at short time scales ($\leq$50 μs).

B. Tubulin and Drugs. MAP-free cow brain tubulin, both unlabeled and labeled with about 2.6 tetramethylrhodamine fluorophores per dimer, was obtained from Molecular Probes. Both were diluted in PIPES buffer (0.1 M PIPES, 1mM $MgCl_2$, pH7.0) supplemented with 0.1 mg/mL BSA. The added BSA reduces the interaction of tubulin with the walls of the sample holder. Without BSA we noticed a loss of the fluorescence intensity with time, as the fluorescent tubulin tends to stick to the walls of the sample holder.

Cryptophycin 1 was a kind gift from Dr. Susan Mooberry, Cancer Research Center of Hawaii. Synthetic hemiasterlin was provided by Dr. Raymond Andersen, University of British Columbia. Dolastatin 10 was supplied by Dr. Robert Schultz, at the Drug Synthesis and Chemistry Branch, National Cancer Institute, Bethesda, Maryland. All other chemicals were purchased from Sigma Chemicals, St. Louis, Missouri, unless otherwise noted.

The drug−tubulin samples were prepared as follows: first relatively high concentrations of tubulin (5 μM) and drug (8 μM) were mixed in the PIPES buffer to initiate ring polymerization and to ensure structural stability as observed and characterized by other techniques (*3*, *4*). Then, the drug−tubulin solution was diluted in PIPES−BSA buffer to a lower nominal concentration (100 nM) and filtered through a 0.22 μm pore filter. At this concentration it is possible to perform FCS measurements. Lower nominal concentration samples were prepared by diluting these primary samples into the same PIPES−BSA buffer. The samples were loaded into 40 μL chambers (Grace Bio-Labs, Inc., Bend, Oregon, USA), which have optically transparent bottom windows made of glass coverslips. This bottom part is in contact with the objective of the inverted microscope (see "FCS Experimental Setup" in this Section). All the experiments were performed at room temperature (22 °C).

C. Cytotoxicity Assays. Human cancer cells used in this study included MCF7 breast carcinoma, PC3 prostate carcinoma, 1A9 ovarian carcinoma, and Ca46 lymphoma and were obtained from the American Type Culture Collection, Manassas, VA. Cells were maintained in culture in RPMI medium with 10% fetal calf serum supplement, at 37 °C with an atmosphere of 5% CO_2 in air. Cytotoxicity testing was performed using the standard sulforhodamine-based protocol, as previously described (*28*). In short, cells were plated in 96-well plates at 10^3 cells per well and exposed to differing concentrations of drugs 1 day after plating. Following 4 days of incubation, cell growth was assessed after fixation and staining with sulforhodamine. IC50 value was taken to be the drug concentration that reduced by 50% the growth after 4 days.

D. Fluorescence Correlation Spectroscopy. In an FCS experiment, temporal fluctuations in fluorescence emission are utilized to obtain information about inter- or intramolecular dynamics or molecular motions occurring on microsecond to second time scales. These fluctuations are induced either by the changes in the number of molecules in the open excitation volume, as they move in and out of the volume, or by changes in the emission quantum yield of the molecules. To obtain high sensitivity, the excitation volume is made small ($\sim$1 fL) either by confocal geometry or by multiphoton excitation (*11*). The time sequence of the detected intensity, $I(t)$, of fluorescence emitted by the fluorescent molecules present in the excitation volume at time, t, is time-correlated to generate a correlation function defined as

$$G(\tau) = 1 + \frac{\langle \delta I(t) \delta I(t+\tau) \rangle}{\langle I(t) \rangle^2} \quad (1)$$

where $\delta I(t) = I(t) - \langle I(t) \rangle$ denotes the spontaneous deviation of the measured intensity from the average intensity, $\langle I(t) \rangle$. Analysis of $G(\tau)$ can provide information about the underlying mechanisms responsible for the intensity fluctuations such as diffusion of the particles, interaction of the particles, and electronic transitions within the molecules.

For an ideal case of freely diffusing monodisperse and uniformly bright fluorescent particles, a closed-form expression of the correlation function, $G(\tau)$, was derived as (*8*)

$$G(\tau) = 1 + \frac{1}{N} \frac{1}{\left(1+\frac{\tau}{\tau_d}\right)} \frac{1}{\left(1 + p\frac{\tau}{\tau_d}\right)^{0.5}} \quad (2)$$

To derive eq 2, it is assumed that the fluorescent particles are excited by a three-dimensional Gaussian beam, whose intensity profile is expressed as

$$W(r,z) = A e^{-2(r/r_o)^2} e^{-2(z/z_o)^2} \quad (3)$$

In eq 3 r_o and z_o define two characteristic sizes: a width of the focused beam spot and a length along the optical axis defined by the direction of the laser beam. Both sizes are used to define the excitation volume, $V = \pi^{3/2} r_o^2 z_o$. With such a Gaussian beam, one identifies a characteristic time, $\tau_d = (r_o)^2/4D$, for fluorescent particles diffusing along the lateral width (r_o) of the focused incident laser beam, D being their translational diffusion coefficient. Also in eq 2, N denotes the average number of particles in the excitation volume, V, and $p = (r_o/z_o)^2$ is an instrumental constant. Further, we apply the Stokes−Einstein relation

$$D = \frac{k_B T}{3\pi\eta d_H} \quad (4)$$

to determine the hydrodynamic diameter, d_H, of the diffusing particles. In eq 4 k_B is the Boltzmann constant, T the temperature of the sample, and η the viscosity of the solvent.

E. Data Analysis. In practice, the analysis of experimental correlation functions (eq 1) is not generally straightforward and depends implicitly on the inherent characteristics of the samples at hand. These samples may contain fluorescent particles which not only are polydisperse in size but also polydisperse in brightness, making it difficult to interpret the measurements (see refs *13* and *29* for discussion). Indeed, like for dynamic light scattering and similar scattering techniques (*30*), extracting the distribution of sizes from the measured FCS correlation functions requires solving a mathematical inverse problem, a challenging task since the problem is ill-posed (*29*, *31*). For example, a group of diffusing particles having three distinctly different sizes might yield a correlation function that is indistinguishable from that deriving from a continuous distribution spanning the same size range. Moreover, for a complete and consistent fitting of the FCS correlations, a priori knowledge of the distribution of brightness of the diffusing fluorescent particles is required. This information cannot be derived from the correlation functions but, rather, must be obtained separately from other measurements such as photon histograms (*13*, *29*). These requirements put some limitations on the technique, as shown by Meseth et al. (*31*), who demonstrated that the resolution limit of FCS depends on several factors including difference in size between particles as well as their concentration and brightness.

The problem of polydispersity of brightness is particularly relevant to the interpretation of our FCS measurements since the tubulin molecules in our stock solutions are not necessarily labeled uniformly. So, instead of the N-value described in eq 2 for uniformly bright particles, it is more appropriate to refer to the limiting factor of the correlation function, $N_{app} = 1/(G(\tau \rightarrow 0) - 1)$, as an "apparent number" of fluorescent particles. For noninteracting particles this quantity is given by (*13*)

$$\frac{1}{N_{app}} = \frac{\sum_i N_i Q_i^2}{[\sum_j N_j Q_j]^2} \quad (5)$$

where N_i is the number of particles of species, i, whose fluorescence quantum yield is Q_i. Because the contribution of each particle, i, to the overall amplitude, $1/N_{app}$, is weighted by Q_i^2, a precise quantification of N_{app} requires a priori characterization of the dispersity in the brightness as mentioned above.

In our case, we avoided possible discrepancies and obtained reliable results by using the same tubulin lot to prepare a primary drug−tubulin solution for each drug at relatively high concentrations of tubulin and drug as described in Materials and Methods. Then, each primary solution was diluted to obtain drug−tubulin samples containing lower concentrations of tubulin and respective drug. As such, the distribution of brightness of the original fluorescent tubulin was likely to have been preserved in all the diluted samples, making it possible to compare N_{app} values between the diluted samples, as well as between the different drug−tubulin samples. In addition to d_H, we monitored the apparent number of fluorescent particles, N_{app}, to obtain information about the stability of the observed polymer entities such as rings and looked for systematic changes of N_{app} as a function of tubulin concentration.

For this paper we simplify by fitting the data with the expression in eq 2 to determine a hydrodynamic diameter, d_H, and an apparent number of fluorescent particles in the excitation volume, $N_{app} = 1/(G(\tau \rightarrow 0) - 1)$. We find that the expression fits well the experimental correlation functions collected from the various drug−tubulin samples (see Results below). It is not our premise that this observation is experimental evidence for the presence of only one particular, monodisperse, structure of tubulin polymer freely diffusing in the solution. In fact (see below), it is likely that some of our samples contain several tubulin polymer structures, including incomplete rings. In this paper the reported hydrodynamic diameter, d_H, merely represents a measure of the principal, average size of the fluorescent particles in the solution. Nonetheless, in many instances we find very good agreement when the experimental d_H is compared with the corresponding diameter calculated from a model of expected structure.

F. FCS Experimental Setup. Our custom FCS instrument utilizes an Olympus IX70 inverted microscope with a 60X,

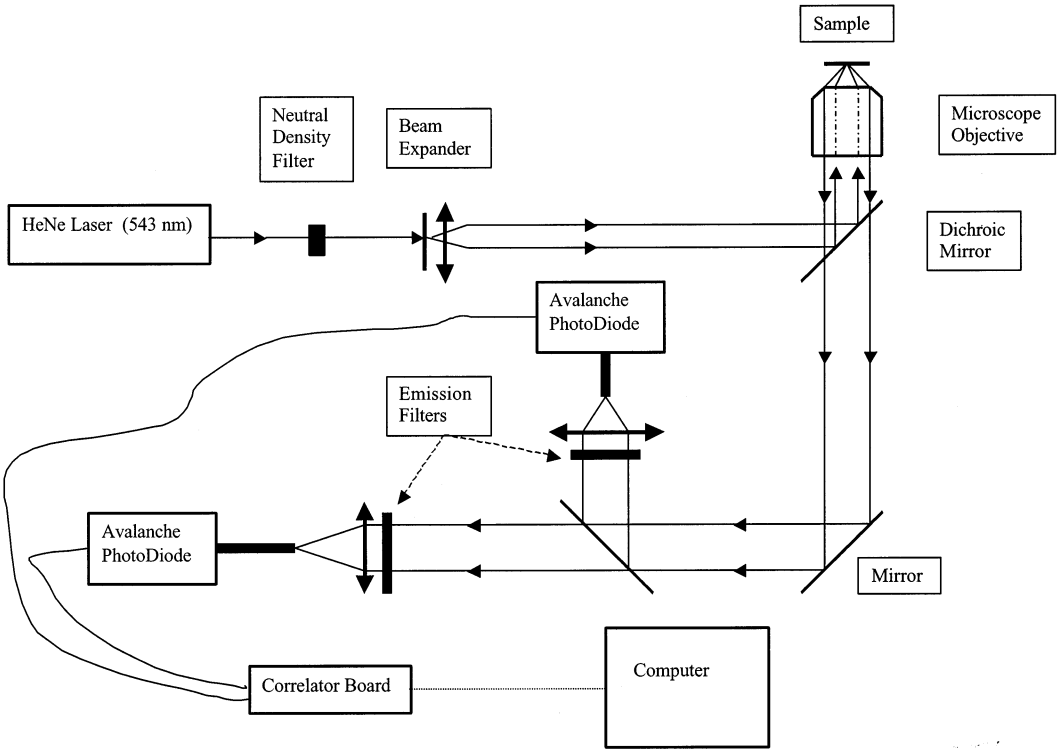

FIGURE 1: Schematic diagram of the FCS setup.

1.2 N.A., water immersion objective and confocal collection optics. In Figure 1 we show a schematic diagram of the experimental setup. For fluorescence excitation, a 1.5 mW 543 nm incident HeNe laser beam (Uniphase, San Jose, California, USA) was first expanded and then focused by the objective onto a small spot with lateral radius ($r_o \approx 1$ μm). However, only a few microWatts of the laser intensity was used in the experiments in order to reduce photobleaching and excitation of molecular triplet states. The emitted fluorescent beam was collected by the same objective and focused onto an optical fiber (OZ Optics, Carp, Ontario, Canada) that has a small core diameter. The small diameter (10 or 25 μm) of the fiber ensures the confocal detection necessary for delimiting the small volumes of interest (*11*). For detection and photocounting, two avalanche photodiodes (SPCM AQ-14, PerkinElmer EG&G, Vaudreuil, Canada) were used in a cross-correlation mode to reduce the effects of spurious detector afterpulsing on the correlation function, which is especially important for short time scales (<10 μs). The pulses of the photodiodes were processed by a digital correlator (BI-9000AT, Brookhaven Instruments Corp., Holtsville, NY) which calculated the correlation function. A built-in cutoff filter was used to remove occasional spurious spikes in the detected signal.

RESULTS

Our results indicate that FCS methods are well suited to investigating the stability of ring polymers of tubulin induced by these drugs. Since the basic data are fluctuations in fluorescence intensity with time, it was essential to control sources of intensity variation other than those due to diffusion of the subject particles. For comparison between the various drug−tubulin samples, we used the average fluorescence intensity in all primary and diluted samples as an indicator of the amount of fluorescent tubulin present in each sample. In addition, because we applied relatively low laser power (≤ 2.6 μW), we did not observe any significant other effects such as triplet transitions or photobleaching. We attribute the measured intensity fluctuations to changes in the number of fluorescent particles diffusing freely in the excitation volume, and fit the measured correlation functions to the expression given by eq 2. FCS data do not easily yield absolute particle numbers or distributions of d_H (see "Data Analysis" in Materials and Methods for a more detailed discussion). Hence, the values obtained from fitting the data are the average hydrodynamic diameter and the apparent number of the fluorescent particles in the excitation volume.

A. Tubulin without Drug (Control). It is important to characterize the original rhodamine-labeled tubulin samples prior to being mixed with any of the drugs. In particular, the dispersity in size of the fluorescent particles needs to be known and, possibly, quantified so that we can compare the measured sizes of the particles present in the original tubulin samples with those of the drug-induced tubulin polymers. In Figure 2 we plot a measured correlation function of a tubulin sample and, for comparison, we include in the same figure the correlation function of a cryptophycin−tubulin sample prepared with tubulin and excess of drug. We also show the correlation function for a sample of rhodamine (TAMRA) diluted in water, used as a standard for calibration. The three correlation functions, which were taken over a 10−30 min period, are normalized to highlight the shift in the time scale due to the increase of the size of the fluorescent particle, rhodamine being the smallest and hence the fastest diffusing particle. More significantly, the figure shows the shift when cryptophycin−tubulin complexes are compared to tubulin alone, indicating an increase in the size of the fluorescent particles following polymerization into tubulin rings. Roughly, the characteristic time, $\tau_{1/2}$, for which $N_{app}(G(\tau) - 1) = 0.5$, of the cryptophycin−tubulin sample

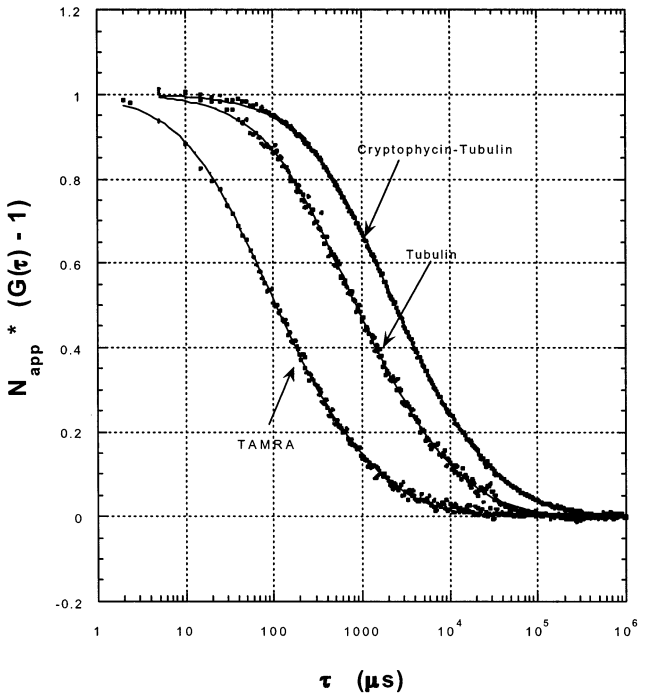

FIGURE 2: Normalized experimental fluorescence correlation curves of rhodamine (TAMRA) used as standard, rhodamine-labeled tubulin, and cryptophycin−tubulin samples, plotted as a function of the delay time, τ. Note the shift in the characteristic time, $\tau_{1/2}$, when cryptophycin is added to the tubulin sample, indicating polymerization of the tubulin dimers into rings (see text and Figures 3a and 4a).

is about 3 times longer than that of the tubulin sample. A fit of the data with the expression given in eq 2 yields $d_H = 6.5 \pm 1$ nm for the tubulin sample, whereas $d_H = 18.9 \pm 1.5$ nm for the cryptophycin−tubulin sample. This result demonstrates that the addition of cryptophycin to the tubulin solution is responsible for the increase in the hydrodynamic diameter, reflecting the polymerized state of the cryptophycin−tubulin compounds.

As pointed out in "Data Analysis" in Materials and Methods, the good fit of the data in Figure 2 with the expression in eq 2 does not imply monodispersity in size and/or brightness of the fluorescent diffusing particles. The d_H value of each sample represents an average value of hydrodynamic diameter of the diffusing fluorescent particles, which can be compared with that derived from an appropriate model. In the case of tubulin, we can model the dimer as a rigid structure composed of two identical spherical beads in contact with each other and calculate the diameter of the beads, d, using the relation $d_H \simeq 1.4d$ (*32*, *33*). From the measured d_H, we calculate $d = 4.7 \pm 0.8$ nm (mean ± S.D, $n = 5$), which, within the experimental error, agrees with the geometrical mean value (4.8 nm) of the known dimensions of the compact ellipsoid shape of tubulin monomer (width ≃ 4.6 nm, height ≃ 4.0 nm, depth ≃ = 6.5 nm) (*34*). We emphasize, though, that this two-bead model is an approximation to the rather nonspherical, asymmetric shape of the actual tubulin monomers. For the cryptophycin−tubulin sample, we further discuss the model in the following Section.

B. Crytophycin−Tubulin Sample. In Figure 3a we plot correlation functions measured from several cryptophycin−tubulin samples. The fluctuating signal was correlated over

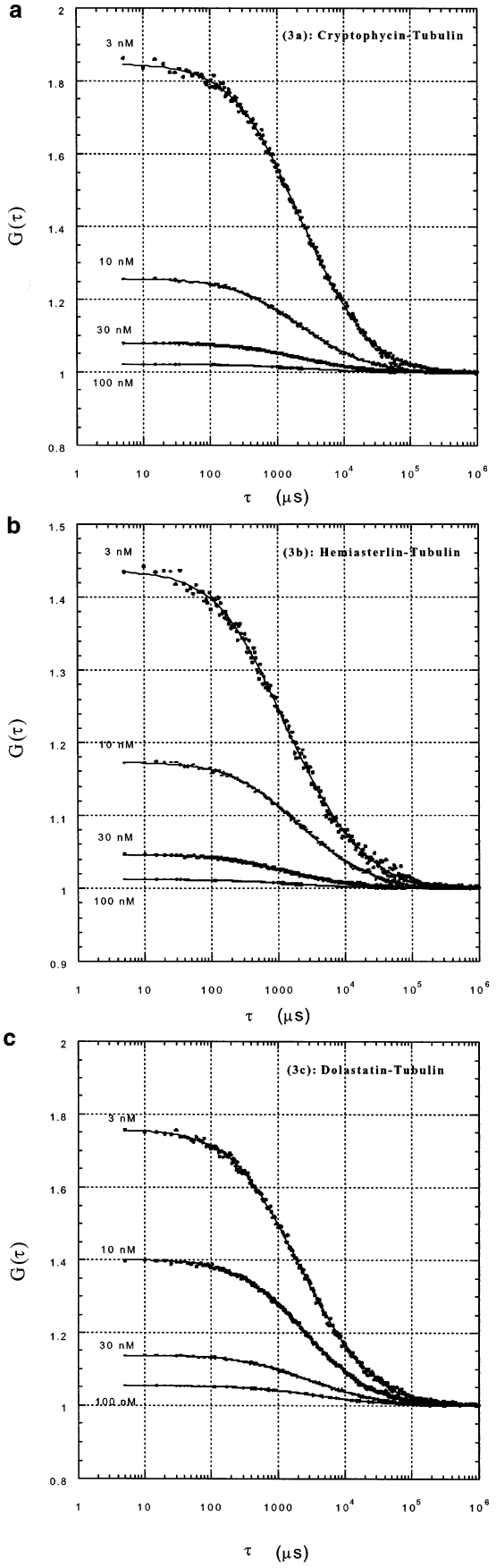

FIGURE 3: Experimental (···) and fitted (−) fluorescence correlation curves of (a) cryptophycin−tubulin, (b) hemiasterlin−tubulin, and (c) dolastatin−tubulin polymers, plotted as a function of delay time, τ. The data are fitted to the expression given in eq 2 (see text). Each curve is labeled with the concentration of the tubulin solution.

a 10−40 min time period depending on the concentration of tubulin. Also in Figure 3a are included the fitting curves of the measured correlation functions. Using the values of r_o and p derived from calibration (see Materials and Methods), we determined two parameters by least-squares fitting the measured correlation functions: the hydrodynamic diameter, d_H, and the apparent number of fluorescent particles, N_{app}.

In Figure 4a, we plot the d_H values for these samples as a function of the tubulin concentration. Note that d_H appears to be independent of tubulin concentration. The mean value of these d_H is 19.8 nm. This measured hydrodynamic diameter can be related to the actual size of the fluorescent particles by choosing an appropriate model for their structure. To analyze the data we used two equivalent approaches. First, we combined the experimental d_H with the known geometry of the cryptophycin−tubulin rings to obtain the actual diameter and, from that, an estimate of the monomer size. Second, we started with the reported diameter of the cryptophycin−tubulin ring and calculated the expected d_H, which we compared with the experimental value.

In approach I we started with the known structure of the rings induced by binding of cryptophycin 1 to tubulin. This is a ring of eight dimers, or 16 monomers. Since α and β tubulin monomers are globular and very close in size we modeled the ring as a rigid ring of 16 identical spherical beads in contact with each other. We calculated the average diffusion coefficient of 16-bead rings of various sizes using the expression derived by Yamakawa and Yamaki (*35*). This analysis indicates that a ring with $d_H = 19.8$ nm (the mean value in Figure 4a) has a diameter of 24.2 nm. This value is very close to the 23.8 nm value obtained by cryo-electron microscopy (Figure 4C of ref *5*). A 24.2 nm ring composed of 16 identical spherical beads also indicates that the diameter of the individual beads is ∼4.7 nm. This is in notable agreement with bead (monomer) size obtained for the tubulin sample alone (see "Tubulin without Drug" above).

In approach II we started with the 23.8 nm diameter ring of beads obtained from cryo-electron microscopy measurements (*5*). Using the method of Yamakawa and Yamaki (*35*), we calculated the hydrodynamic diameter to be $d_{cal} = 19.2$, which is shown as a solid line in Figure 4a. We did a similar calculation using the HYDRO protocol of de la Torre et al. (*32*, *33*) and obtained a value of $d_{cal} = 19.04$ nm. Both calculated values are very similar and are similar to the experimental value, $d_H = 19.8$ nm. Thus, by both approaches I and II, the average value obtained for d_H of the cryptophycin−tubulin complexes is consistent with a 23.8 nm diameter ring composed of 16 identical beads of ∼4.6 nm diameter.

Since this value is obtained even after significant dilution (Figure 4a), these results indicate that the ring geometry is stable even at tubulin concentrations as low as 1 nM, and for at least the 6 h period of the experimental run. Had the cryptophycin−tubulin rings depolymerized, a shift of the apparent size to lower values would have been observed.

A consistent result can be obtained by analyzing the change of the apparent number of fluorescent particles, N_{app}, as a function of the tubulin concentration. In Figure 5, we plot N_{app} as a function of the tubulin concentration for the cryptophycin−tubulin samples, as well as for the hemiasterlin−tubulin and dolastatin−tubulin samples discussed below.

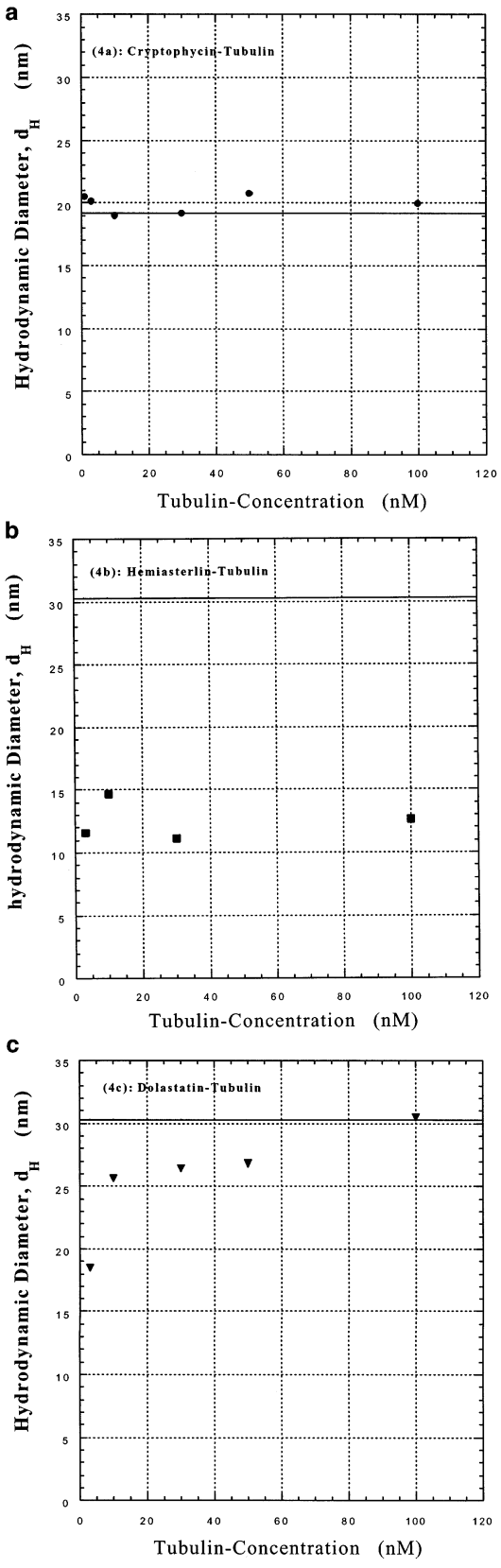

FIGURE 4: The hydrodynamic diameter of the fluorescent polymer structures determined from FCS correlation functions obtained from (a) cryptophycin−tubulin, (b) hemiasterlin−tubulin, and (c) dolastatin−tubulin, shown as a function of the tubulin concentration. In all samples the ratio of drug to tubulin was kept constant, [Drug]/[Tubulin] = 1.3. The solid lines are the calculated hydrodynamic diameters of the stable rings, which were characterized by other techniques using relatively high concentrations of tubulin (>5 μM). The results indicate that the rings are differentially stable to dilution.

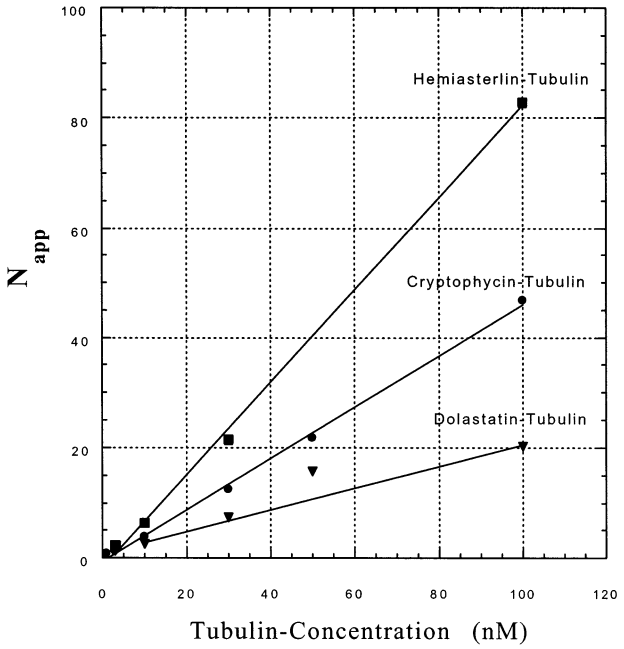

FIGURE 5: The apparent number of fluorescent particles determined from fitting eq 2 to measured FCS correlation functions, plotted as a function of the tubulin concentration. In all samples the ratio of drug to tubulin was kept constant, [Drug]/[Tubulin] = 1.3. Note that the observed number of fluorescent particles in the hemiasterlin−tubulin samples is larger than that of cryptophycin−tubulin sample, contrary to what is expected for the larger size of hemiasterlin−tubulin rings (see text). A straight line with zero intercept implies dilution without dissociation in this concentration range. Cryptophycin rings show this behavior. Dilution with dissociation will result in more complex behavior. While we draw a straight line for the dolastatin data, the increase of N_{app} compared to cryptophycin at concentrations < 10 nM indicates dissociation of the dolastatin rings (see Figure 4c and discussion in the text).

In cryptophycin−tubulin samples, we notice what appears to be a linear dependence of N_{app} on the tubulin concentration. As with the behavior of d_H, this is another strong indication of the stability of the rings.

C. Hemiasterlin−Tubulin Sample. Similarly to the cryptophycin−tubulin samples, we measured and fitted the correlation functions obtained from the hemiasterlin−tubulin samples. In Figure 3b we show some measured and fitted correlation functions obtained from several samples prepared with different tubulin concentrations. In Figure 4b we plot the hydrodynamic diameter as a function of the tubulin concentration and, for comparison, include the calculated hydrodynamic diameter for stable hemiasterlin−tubulin rings derived from the bead ring model with 28 × 4.7 nm beads (d_H = 30.3 nm (*35*), d_H = 29.7 nm (*33*)). Noticeably, FCS measurements of the hemiasterlin−tubulin samples show a different stability behavior than those of cryptophycin−tubulin samples. Instead of the expected ring diameter, the measured d_H is much smaller. This suggests that the rings depolymerized into smaller fluorescent entities. To make sure that complete hemiasterlin−tubulin rings did, indeed, form before depolymerizing upon dilution, we prepared a hemiasterlin−tubulin sample containing 50 nM of rhodamine-labeled and 4.95 μM unlabeled tubulin mixed with 8 μM concentration of hemiasterlin. The relatively high total concentration of tubulin (5 μM) ensured the formation and stability of the rings, while the small amount of labeled tubulin allowed us to measure the correlation functions of the sample. Though not shown in Figure 4b, we determined the hydrodynamic diameters of these fluorescent particles to be close to the known diameter for stable hemiasterlin−tubulin rings.

An additional result consistent with the observation of depolymerization of hemiasterlin−tubulin rings (≤100 nM) can be drawn from analysis of the apparent number of particles, N_{app}, shown in Figure 5. When compared at a given tubulin concentration, the value N_{app} of the hemiasterlin−tubulin sample is larger than that of the cryptophycin−tubulin sample. This is contrary to the results expected for stable hemiasterlin−tubulin rings. That is, if the hemiasterlin−tubulin rings were stable, one should have observed a smaller number of particles than that seen in the corresponding cryptophycin−tubulin solution, since complete hemiasterlin−tubulin rings contain 14 tubulin dimers whereas cryptophycin−tubulin rings are formed with 8 dimers (recall that the total concentration of tubulin in the solutions is the same.) It is possible to estimate the average number of tubulin dimers in the hemiasterlin−tubulin polymers by comparing the slopes of the linear dependencies of N_{app} as a function of the tubulin concentration. If, as indicated above, we attribute the cryptophycin−tubulin curve to stable rings composed of eight dimers, the ratio of the slopes of the hemiasterlin−tubulin and cryptophycin−tubulin curves implies that the average number of dimers in the hemiasterlin−tubulin polymers is 3.13, close to 3. It is not clear what structure these 3 dimers have formed. However, if we assume a collinear hexamer (6 rigid beads of 4.7 nm diameter), we calculate d_H to be 11.8 nm (*32*, *33*), which is very close to the average value of 12.5 nm of the measured hydrodynamic diameter (see Figure 4b).

D. Dolastatin−Tubulin Sample. In contrast to the cryptophycin−tubulin and hemiasterlin−tubulin samples, the dolastatin−tubulin samples show an intermediate stability behavior. In Figure 3c we plot measured and fitted correlation functions obtained from some of the dolastatin−tubulin samples. Similarly, we show in Figure 4c the hydrodynamic diameters determined from the measured correlation functions and the expected hydrodynamic diameter calculated from the known size of the stable dolastatin−tubulin rings using the bead ring model with 28 × 4.7 nm beads (d_H = 30.3 nm (*35*), d_H = 29.7 nm (*33*)). Although the measured hydrodynamic diameters indicate a tendency of the dolastatin−tubulin rings to depolymerize, it is only at a rather low concentration ([Tubulin] < 10 nM) that a significant change is observed in the hydrodynamic size. In addition, at the lowest (3 nM) tubulin concentration, we observed a systematic decrease in the apparent hydrodynamic diameter with time following the preparation of the sample (data not shown.)

As expected, at sufficiently high concentration, the apparent number of fluorescent particles in the dolastatin−tubulin solution is lower than that in the corresponding cryptophycin−tubulin sample (see Figure 5). Indeed, given the known numbers of tubulin dimers in dolastatin−tubulin rings (viz., 14) and cryptophycin−tubulin rings (viz., 8), the ratio between the concentration of cryptophycin−tubulin rings and that of dolastatin−tubulin rings should be 14/8 = 1.75 for identical concentrations of tubulin. As calculated from the data, the ratio N_{app} for cryptophycin−tubulin to N_{app}

Table 1: Cytotoxicity of Various Peptide Drugs on Different Cell Lines. We List the Values, Expressed in Nanomolar, of the Drug Concentration (IC50) that Reduces by 50% the Rate of Cell Growth after 4 days of Incubation

drug	1A9	PC3	Ca46	MCF7
cryptophycin 1	0.01	0.016	0.012	0.01
dolastatin 10	0.05	0.08	0.06	0.04
hemiasterlin	0.24	0.6	0.2	0.3
vinblastine	1.1	1.9	1.1	1
taxol	5	8	6	6

for dolastatin−tubulin varies between 1.4 and 2.3 for tubulin concentrations larger than 3 nM, consistent with the expected value. That is, more fluorescent particles are present in the cryptophycin−tubulin sample than that of its corresponding dolastatin−tubulin one. (The variation in the value of the ratio can be attributed to slight but significant differences in the tubulin concentration following the preparation, filtering, and dilution of the samples, and to the depolymerization trend of the rings as suggested by the measured hydrodynamic diameter, see Figure 4c). For 3 nM tubulin concentration, where d_H of the dolastatin−tubulin sample has significantly decreased, the ratio falls below 1, another indicator of significant depolymerization of the tubulin polymers into smaller entities. Overall, the fact that the ratio of the number of cryptophycin−tubulin rings to that of dolastatin−tubulin rings is generally close to the expected value of 1.75, whereas the ratio for the cryptophycin−tubulin to hemisasterlin−tubulin is less than 1 over all tubulin concentrations, indicates that dolastatin−tubulin rings are much more stable than hemiasterlin−tubulin rings.

E. Cell Culture and Cytotoxicity Measurements. The principal focus of this study was to examine differences in the stabilities of the ring polymers induced by these different agents. However, antitubulin agents are also known to vary considerably in cytotoxic potency. Therefore, we also compared the relative cytotoxities of these agents. We wished to compare these agents in side-by-side assays with the same test cells, and to compare the results relative to the stabilities found by FCS.

In Table 1 we list the IC50 values derived for the different cell lines using the drugs studied here (cryptophycin, hemiasterlin, and dolastatin.) For comparison we include the IC50 values of reference drugs, taxol and vinblastine. We first notice the high level of cytotoxicity of the drugs when compared with taxol or vinblastine. Second, when compared with each other, cryptophycin appears to be the most toxic, followed by dolastatin and hemiasterlin. Interestingly, this trend in the drug cytotoxicity correlates rather well with the stability of the rings.

SUMMARY

A primary interest in Fluorescence Correlation Spectroscopy (FCS) is its suitability for applications to solutions of nanomolar concentrations of fluorescent probes. The technique is particularly attractive in situations requiring the use of small quantities of costly or rare materials. In this study, we successfully applied FCS to measure the translational diffusion coefficient of rhodamine-labeled tubulin dimers, as well as parameters of drug-induced tubulin polymers. More importantly, we determined and monitored changes in the measured translational diffusion coefficient and the apparent number of fluorescent particles as the concentration of tubulin was lowered to the nanomolar range.

Table 2: Comparison of the Sizes Measured by FCS and Other Techniques

	measured d_H by FCS (nm)	inferred size from d_H based on shape[a] (nm)	diameter of stable rings[e] (nm)
cryptophycin−tubulin	19.8 ± 2	24.2 ± 3[b]	23.8
hemiasterlin−tubulin	12.5 ± 2	incomplete rings[c]	44.6
dolastatin−tubulin [tub] > 10 nM	28.0 ± 3	38.8 ± 4.6[d]	44.6
dolastatin−tubulin [tub] = 3 nM	18.0 ± 2	incomplete rings	44.6

[a] The calculated diameters are inferred from the measured hydrodynamic diameter, d_H, by modeling the structure as a rigid bead ring made of a number, m, of 4.7 nm beads (see text and (*35*).) [b] The number of beads: $m = 16$. [c] The structure of the depolymerized hemiasterlin−tubulin rings is not known. It is likely to be composed of three tubulin dimers, which can be modeled as linear hexamers of 4.7 nm beads (see text.). [d] The number of beads: $m = 28$. [e] The diameter of the stable rings was determined previously by other techniques (DLS, EM, ...) (see refs *3*−*5*.)

Three drugs—cryptophycin, hemiasterlin, and dolastatin—were studied. Table 2 summarizes the results of the FCS measurements on samples of various concentrations. At relatively high concentrations (>1 μM), results obtained from other techniques (electron microscopy, dynamic light scattering, and ultracentrifugation) suggest that the main polymer structure is a single-walled ring with mean diameter ranging from 23.8 (cryptophycin) to 44.6 nm (hemiasterlin and dolastatin). As the concentration of tubulin is lowered, FCS measurements on these drug-induced tubulin rings at room temperature reveal different levels of stability of the rings. With cryptophycin, the FCS measurements indicate that the rings are very stable: no depolymerization was observed in samples of nanomolar tubulin concentrations. In hemiasterlin−tubulin samples, the rings depolymerized even at 100 nM tubulin concentration. However, the dolastatin−tubulin samples show an intermediate level of stability; only at low tubulin concentration ($\leq$ 10 nM) was significant depolymerization observed.

The in vitro stability of the drug−tubulin rings appears to roughly correlate with the cytotoxicity of the drugs in different cell lines. Indeed, Table 1 indicates that cryptophycin is the most potent cytotoxic drug, followed by dolastatin and hemiasterlin in the same order as the stability of ring structures indicated by the FCS data shown in Figures 4 and 5. This result corroborates that of Lobert et al. (*36*), who investigated a class of C-20′ modified vinca alkaloid congeners and discovered a strong correlation between the ability of a compound to induce the formation of tubulin spirals and its cytotoxicity against a leukemic cell line, L1210. However, we are not proposing that the cytotoxicity of these agents is due to bulk conversion of cellular tubulin into the drug−tubulin ring polymers studied here. Previous studies (*20*, *37*) of cellular uptake of cryptophycin and dolastatin reveal that, at concentrations near the IC50, these drugs are concentrated intracellularly manyfold over the extracellular concentration. Yet, the resulting intracellular concentration is still much lower (as much as 1000-fold) than the total cellular tubulin concentration. This is quite different from the slight stoichiometric excess of drug over tubulin used in our studies, and indicates that cytotoxicity is likely

due to drug mediated disruption of microtubule dynamics as suggested in those studies (*20*, *37*), rather than massive conversion of tubulin to the ring form. We plan further studies of drug−tubulin interaction at substoichiometric ratios of drug to tubulin, to address the question of cooperativity of ring formation and, consequently, the possible role of ring formation in the mechanism of cytotoxicity.

REFERENCES

1. Dumontet, C. and Sikic, B. I. (1999) Mechanisms of Action of and Resistance to Antitubulin Agents: Microtubule Dynamics, Drug Transport, and Cell Death, *J. Clin. Oncol. 17*, 1061−1070.
2. Hamel, E., and Covell, D. G. (2002) Antimitotic Peptides and Depsipeptides, *Curr. Med. Chem. − Anticancer Agents 2*, 19−53.
3. Bai, R., Taylor, G. F., Schmidt, J. M., Williams, M. D., Kepler, J. A., Pettit, G. R., and Hamel, E. (1995) Interaction of Dolastatin 10 with Tubulin: Induction of Aggregation and Binding and Dissociation Reactions, *Mol. Pharmacol. 47*, 965−976.
4. Watts, N. R., Sackett, D. L., Ward, R. D., Miller, M. W., Wingfield, P. T., Stahl, S. S., and Steven, A. C. (2000) HIV-1 Rev Depolymerizes Microtubules to Form Stable Bilayered Rings, *J. Cell Biol. 150*, 349−360.
5. Watts, N. R., Cheng, N., West W., Steven, A. C., and Sackett, D. L. (2002) The Cryptophycin-Tubulin Ring Structure Indicates Two Points of Curvature in the Tubulin Dimer, *Biochemistry 41*, 12662−12669.
6. Elson, E. L., and Magde, D. (1974) Fluorescence Correlation Spectroscopy: I. Conceptual Basis and Theory, *Biopolymers 13*, 1−27.
7. Magde, D., Elson, E. L., and Webb W. W. (1974) Fluorescence Correlation Spectroscopy: II. An Experimental Realization, *Biopolymers 13*, 29−61.
8. Aragon, S. R., and Pecora, R. (1976) Fluorescence Correlation Spectroscopy *J. Chem. Phys. 64*, 1792−1803.
9. Rigler, R., Mets, Ü., Widengren, J., and Kask, P. (1993) Fluorescence Correlation Spectroscopy with High Count Rate and Low Background: Analysis of Translational Diffusion, *Eur. Biophys. J. 22*, 169−175.
10. Chen, Y., Müller, J. D., Berland, K. M., and Gratton, E. (1999) Fluorescence Fluctuation Spectroscopy, *Methods 19*, 234−252.
11. Webb, W. W. (2001) Fluorescence Correlation Spectroscopy: Inception, Biophysical Experimentations, and Prospectus, *Appl. Opt. 40*, 3969−3983.
12. Rigler, R., and Elson, E. S., Eds. (2001) In *Fluorescence Correlation Spectroscopy: Theory and Applications*, Springer Series in Chemical Physics, Springer-Verlag, New York.
13. Krichevsky, O., and Bonnet, G. (2002) Fluorescence Correlation Spectroscopy: the Technique and its Applications, *Rep. Prog. Phys. 65*, 251−297.
14. Craencenbroeck, E. V., and Engelborghs, Y. (1999) Quantitative Characterization of the Binding of Fluorescently Labeled Colchicine to Tubulin in vitro using Fluorescence Correlation Spectroscopy, *Biochemistry 38*, 5082−5088.
15. Neumann, T., Kirschstein, S. O., Gomez, J. A. C., Kittler, L., and Unger, E. (2001) Determination of the Net Exchange Rate of Tubulin Dimer in Steady-State Microtubules by Fluorescence Correlation Spectroscopy, *Biol. Chem. 382*, 387−391.
16. Schwartz, R. E., Hirsch, C. F., Sesin, D. F., Flor, J. E., Chartrain, M., Fromtling, R. E., Harris, G. H., Salvatore, M. J., Liesch, J. M., Yudin, K. (1990) Pharmaceuticals from Cultured Algae, *J. Indust. Microbiol. 5*, 113−123.
17. Smith, C. D., Zhang, X., Mooberry, S. L., Patterson, G. M. L., and Moore, R. E. (1994) Cryptophycin: a New Antimicrotubule Agent Active Against Drug-Resistant Cells, *Cancer Res. 54*, 3779−3784.
18. Bai, R., Schwartz, R. E., Kepler, J. A., Pettit, G. R., and Hamel, E. (1996) Characterization of the Interaction of Cryptophycin 1 with Tubulin: Binding in the Vinca Domain, Competitive Inhibition of Dolastatin 10 Binding, and an Unusual Aggregation Reaction, *Cancer Res. 56*, 4398−4406.
19. Panda, D., Himes, R. H., Moore, R. H., Wilson, L., and Jordan, M. A. (1997) Mechanism of Action of the Unusually Potent Microtubule Inhibitor Cryptophycin 1, *Biochemistry 36*, 12948−12953.
20. Panda, D., Deluca, K., Williams, D., Jordan, M. A., and Wilson, L. (1998) Antiproliferative Mechanism of Action of Cryptophycin 52: Kinetic Stabilization of Microtubule Dynamics by High Affinity Binding to Microtubule Ends, *Proc. Natl. Acad. Sci. U.S.A.* 95, 9313−9318.
21. Talpir, R., Benayahu, Y., Kashman, Y., Pannell, L., and Schleyer, M. (1995) Hemiasterlin and Geodiamolide TA.; Two New Cytotoxic Peptides from the Marine Sponge Hemiasterella Minor (Kirkpatrick), *Tetrahedron Lett. 35*, 4453−4456.
22. Coleman, J. E., Patrick, B. O., Andersen, R. J., and Allen, T. M. (1995) Cytotoxic Peptides from the Marine Sponge Cymbaslela-sp., *Tetrahedron 51*, 10653−10662.
23. Gamble, W. R., Durso, N. A., Fuller, R. W., Westergaard, C. K., Johnson, T. R., Sackett, D. L., Hamel, E., Cardellina II, J. H., and Boyd, M. R. (1999) Cytotoxic and Tubulin-Interactive Hemiasterlins from Auletta sp. and Siphonochalina spp- Sponges, *Bioorg. Med. Chem. 7*, 1611−1615.
24. Bai, R., Durso, N. A., Sackett, D. L., and Hamel, E. (1999) Interactions of Sponge-Derived Antimitotic Tripeptide Hemiasterlin with Tubulin. Comparison with Dolastatin 10 and Cryptophycin 1, *Biochemistry 38*, 14302−14310.
25. Pettit, G. R., Kamano, Y., Herald, C. L., Tuinman, A. A., Boettner, F. E., Kizu, H., Schmidt, J. M., Baczynskyj, L., Tomer, K. B., and Bontems, R. J. (1987) Antineoplastic Agents 136. The Isolation and Structure of a Remarkable Marine Animal Antineoplastic Constituent -Dolastatin 10, *J. Am. Chem. Soc. 109*, 6883−6885.
26. Bai, R., Taylor, G. F., Cichacz, Z. A., Herald, C. L., Kepler, J. A., Pettit, G. R., and Hamel, E. (1995) The Spongistatins, Potently Cytotoxic Inhibitors of Tubulin Polymerization, Bind in a Distinct Region of the Vinca Domain, *Biochemistry 34*, 9714−9721.
27. Bai, R., Pettit, G. R., and Hamel, E. (1990) Dolastatin-10, a Powerful Cytostatic Peptide Derived from a Marine Animal-Inhibition of Tubulin Polymerization Mediated through the Vinca Alkaloid Binding Domain, *Biochem. Pharmacol. 39*, 1941−1949.
28. Skehan, P., Storeng, R., Scudiero, D., Monks, A., McMahon, J., Vistica, D., Warren, J. T., Bokesch, H., Kenney, S., and Boyd, M. R. (1990) New Colorimetric Cytotoxicity Assay for Anticancer-Drug Screening, *J. Natl. Cancer Inst. 82*, 1107−1112.
29. Starchev, K., Buffle, J., and Pérez, E. (1999) Applications of Fluorescence Correlation Spectroscopy: Polydispersity Measurements, *J. Colloid Interface Sci. 213*, 479−487.
30. Chen, S.-H., Chu, B., and Nossal, R., Eds. (1981) In *Scattering Techniques Applied to Supramolecular and Nonequilibrium Systems*, NATO Advanced Study Institutes Series B, Vol. 73, Plenum Press, New York.
31. Meseth, U., Wohland, T., Rigler, R., and Vogel, H. (1999) Resolution of Fluorescence Correlation Measurements, *Biophys. J. 76*, 1619−1631.
32. de La Torre, J. G., and Bloomfield, V. A. (1981) Hydrodynamic Properties of Complex, Rigid, Biological Macromolecules: Theory and Applications, *Q. Rev. Biophys. 14*, 81−139.
33. de La Torre, J. G., Navarro, S., Martinez, M. C. L., Diaz, F. G., and Cascales, J. L. (1994) HYDRO: A Computer Software for the Prediction of Hydrodynamic Properties of Macromolecules, *Biophys. J. 67*, 530−531.
34. Nogales, E., Whittaker, M., Milligan, R. A., and Downing, K. H. (1999) High-Resolution Model of the Microtubule, *Cell 96*, 79−88.
35. Yamakawa, H., and Yamaki, J. I. (1973) Application of the Kirkwood Theory of Transport in Polymer Solutions to Rigid Assemblies of Beads, *J. Chem. Phys. 58*, 2049−2055.
36. Lobert, S., Fahy, J., Hill, B. T., Duflos, A., Etievant, C., and Correia, J. J. (2000) Vinca Alkaloid-Induced Tubulin Spiral Formation Correlates with Cytotoxicity in the Leukemic L1210 Cell Line, *Biochemistry 39*, 12053−12062.
37. Verdier-Pinard, P., Kepler, J. A., Pettit, G. R., and Hamel, E. (2000) Sustained Intracellular Retention of Dolastatin 10 Causes its Potent Antimitotic Activity, *Mol. Pharmacol. 57*, 180−187.

BI026751Q